



Title	Direct measurement of magnetocaloric effect (MCE) in frustrated Gd-based molecular complexes
Author(s)	Zhang, Yu; Nomoto, Tetsuya; Yamashita, Satoshi et al.
Citation	Journal of Thermal Analysis and Calorimetry. 2024
Version Type	VoR
URL	https://hdl.handle.net/11094/98269
rights	This article is licensed under a Creative Commons Attribution 4.0 International License.
Note	

The University of Osaka Institutional Knowledge Archive : OUKA

<https://ir.library.osaka-u.ac.jp/>

The University of Osaka



Direct measurement of magnetocaloric effect (MCE) in frustrated Gd-based molecular complexes

Yu Zhang¹ · Tetsuya Nomoto² · Satoshi Yamashita¹ · Hiroki Akutsu¹ · Nobuto Yoshinari¹ · Takumi Konno¹ · Yasuhiro Nakazawa¹

Received: 29 November 2023 / Accepted: 21 May 2024
© The Author(s) 2024

Abstract

Generation of low temperatures below 1 K has been required for applications and fundamental research, given this, development of new materials utilized for demagnetization cooling has extensively been performed in recent years. Here, we studied two polynuclear Gd³⁺-based molecular compounds of Gd_{0.33}[Gd₄(OH)₄(OAc)₃][Rh₄Zn₄(L-cys)₁₂]·32H₂O (**1**_{Gd}) and Gd_{0.33}[Gd₄(OH)₄(OAc)₃][Ir₄Zn₄(L-cys)₁₂]·28H₂O (**2**_{Gd}) (L-cys = L-cysteinate) which show paramagnetic even at low temperatures due to their frustrated arrangement of Gd³⁺ ions. We discuss the magnitude of the magnetocaloric effect (MCE) in them inferred from the isothermal magnetic entropy change (ΔS_M) from isothermal magnetization data. The $-\Delta S_M^{\max}$ of **1**_{Gd} and **2**_{Gd} are 15.15 J kg⁻¹ K⁻¹ and 17.49 J kg⁻¹ K⁻¹ occur at 2.0 K under an applied field from 0 to 7 T, respectively. We also discussed the results of heat capacity measurement under magnetic fields to confirm the validity of the entropy change for **1**_{Gd}. Furthermore, with an aim of detecting their MCE directly, we have developed a new non-magnetic and metal-free magnetocaloric measurement cell. The adiabatic temperature change (ΔT_{ad}) occurs in a small amount of sample on an order of 10²-microgram with the application and removal of various magnitude magnetic fields starting from several initial temperatures were detected directly, to evaluate the potential of them to be a refrigerant for an adiabatic demagnetization refrigerator. The instrumental design for direct measurements of MCE is described along with the construction details.

Keywords Magnetocaloric effect · Molecular refrigerant · Gadolinium · Cubane · Frustrated

Introduction

Increasing interests and demand for achieving extremely low temperatures below the liquid helium temperature region using a handy cryostat are rapidly expanding both in science and engineering. This growth is driven by the promising usage of quantum computing, nano-dot devices, etc. operating under low-energy and precise conditions. Promoting the development of refrigeration systems that can work at low cost and sustainably has become essential for cryogenic industry for handling these new quantum techniques [1]. Magnetic refrigeration is an emerging, low-cost, environment-friendly technology based on the magnetocaloric effect

(MCE). Nominally, MCE is a magneto-thermodynamic phenomenon that manifests a change in material temperature through entropy change induced by a change in an external applied magnetic field under adiabatic conditions. The alignment of spin directions and their redistribution by the release of internal energy induced by magnetic fields lead to changes in adiabatic temperature [2–6]. From the scientific viewpoint, MCE can probe interactions between spins and other degrees of freedom for example phonons in crystal lattices. These phenomena are utilized for making drastic changes in temperatures only by varying external magnetic fields [7]. In fact, without using ³He and ³He-⁴He mixture gas, it is possible to get cryostat available temperatures below the liquid helium range where the quantum sciences and their technology become realistic.

As for the materials to give MCE, ferromagnetic materials including transition metals Fe or Co are widely performed because of their high spin states with large magnetic moments resulting in entropy shift up to the higher temperature side upon applying a magnetic field giving favorable

✉ Yu Zhang
zhangy22@chem.sci.osaka-u.ac.jp

¹ Department of Chemistry, Graduate School of Science, Osaka University, Toyonaka, Osaka 560-0043, Japan

² Institute for Solid State Physics, The University of Tokyo, Kashiwa, Chiba 277-8581, Japan

situation for MCE [8–10]. In particular, cubic Laves phase (AB₂) materials such as ZrFe₂, GdCo₂, etc. have been typically studied for adiabatic demagnetization coolers [8, 9, 11–16]. And the B-doped La(Fe_xSi_{1-x})₁₃B_y are used as room temperature magneto-cooling materials [10, 17–19]. Compounds with Gd³⁺ ions offer advantages for giving large magnetocaloric effects since Gd³⁺ is 4f⁷ configuration with unpaired electrons spin without possessing orbital quantum numbers [20, 21]. Notably, ferromagnetic material such as Gd₅(Si_xGe_{1-x})₄ [2], have been extensively studied near room temperature to produce giant magnetocaloric effects [22–26], and still serves as a reference material. It is more recently suggested that the crystals of polynuclear metal complexes or coordination polymers of Gd³⁺ with organic ligands can attain large MCE powers to reach extremely low temperatures since the high degeneracy of spin levels in 4f⁷ of Gd³⁺ ions can generate paramagnetic MCE through the Zeeman splitting. According to previous reports, extensive studies of molecules-based compounds aiming to achieve cooling applications at ultra-low temperatures have emerged, as their MCE can be larger than that observed in the best intermetallics and alloys [27–30]. A molecular magneto-cooling material reported by Roubeau et al. [31] shows large magnetic entropy change of $-\Delta S_M^{\max} = 40.0 \text{ J kg}^{-1} \text{ K}^{-1}$ at $T = 1.8 \text{ K}$ at $\Delta H = 7 \text{ T}$. Furthermore, higher performances have been investigated in polynuclear cluster complexes of Gd³⁺ for getting cryocooling materials. Luo et al. [32] have synthesized a large lanthanide-exclusive cluster complex of [Gd₆₀(CO₃)₈(CH₃COO)₁₂(μ₂-OH)₂₄(μ₃-OH)₉₆(H₂O)₅₆](NO₃)₁₅Br₁₂(dmp)₅·30CH₃OH·20Hdmp (1-Gd₆₀), the $-\Delta S_M^{\max}$ of it is $48.0 \text{ J kg}^{-1} \text{ K}^{-1}$ at 2 K for $\Delta H = 7 \text{ T}$, which is quite large among reported high-nuclearity lanthanide clusters.

For obtaining good cooling power in these molecules-based magnetic materials, it is necessary to reduce interactions between neighboring spins which tend to show antiferromagnetic behaviors due to the superexchange type mechanism [33, 34]. Furthermore, the introduction of organic ligands works to decrease the density of magnetic ions compared with intermetallic compounds that sometimes become an obstacle to dense assembly of Gd³⁺ ions in a crystal. These are contradictory conditions and compete with each other in designing Gd³⁺-based molecular cooling materials. Introducing frustrated structures into the polynuclear cluster units can be a kind of solution for this problem since the strong frustrations prohibit the formation of ordering and then keep paramagnetic states down to low temperature.

Here, we focus on a system of Gd-cluster system of cubane-based coordination polymer materials. Crystals of Gd_{0.33}[Gd₄(OH)₄(OAc)₃][Rh₄Zn₄(L-cys)₁₂]·32H₂O (**1**_{Gd}) and Gd_{0.33}[Gd₄(OH)₄(OAc)₃][Ir₄Zn₄(L-cys)₁₂]·28H₂O (**2**_{Gd}) (L-cys = L-cysteinate) were prepared by Yoshinari et al. by single-crystal to single-crystal method [35]. They successfully introduced a tetranuclear cubane-type

Gd-cluster into a metallo-supramolecular framework, wherein the Gd³⁺ ions form a triangle shape within the cubane structure resulting in geometric frustration that weakens the internal correlation between Gd metal ions [36–38]. Although the neighboring Gd-Gd distance is much closer than other Gd-cluster compounds, they do not show long-range ordering due to the frustration forms from the cubane. Using the newly constructed apparatus, we directly measured the MCE and compared the results with those of magnetic susceptibility and the heat capacity measurements under magnetic fields.

Experimental

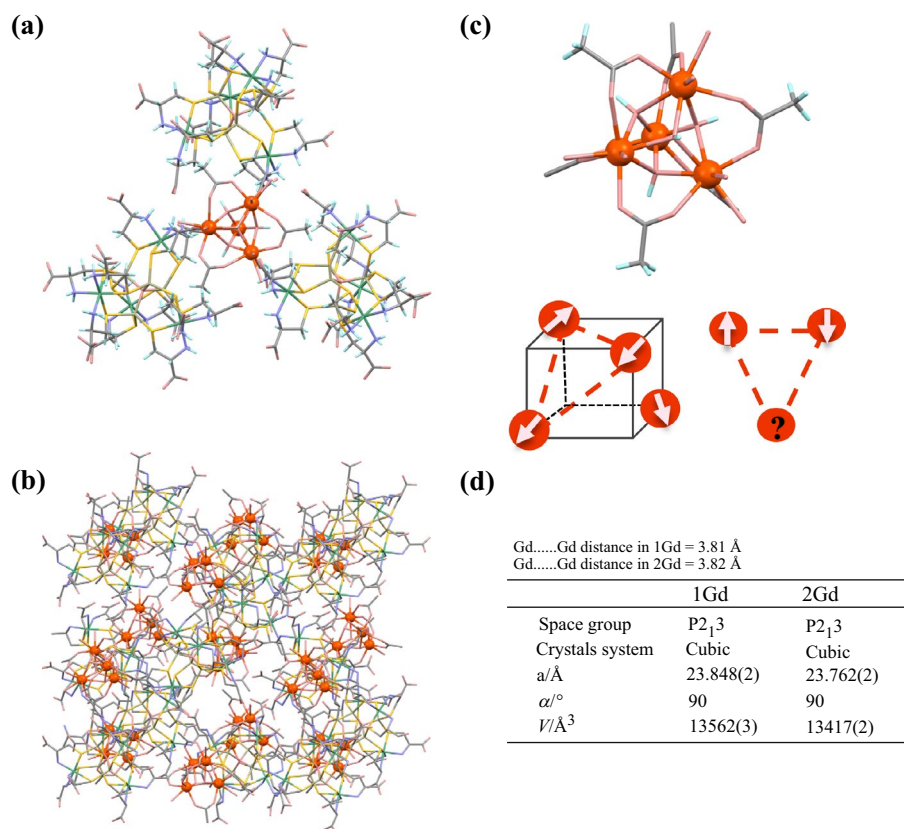
The crystal structure of the compounds **1**_{Gd} and **2**_{Gd} are shown in Fig. 1. The synthetic details of the anionic framework of [Rh₄Zn₄(L-cys)₁₂]⁶⁻ are as reported in Ref. [35] and replacements of counter cations from hydrated Li⁺, K⁺, Cs⁺ ions to Gd³⁺ are also illustrated in the literature. The peculiar structural feature of these compounds is that Gd³⁺ ions form a cubane cluster in the main frameworks. The neighboring Gd-Gd distance in each material is 3.81 Å and 3.82 Å, respectively, which are relatively smaller than those of other molecular clusters mentioned in the introduction, the formation of cubane network may form a frustrated structure.

The temperature dependence of magnetic susceptibility and isothermal magnetization measurements for **1**_{Gd} and **2**_{Gd} were performed by a commercial Magnetic Property Measurement System (MPMS) XL system. The data of isothermal magnetization were collected between 2 and 10 K up to the maximum magnetic field of 7 T. The sample mass of **1**_{Gd} and **2**_{Gd} is 10.2385 mg and 20.0760 mg, respectively. MCE can be effectively estimated with the isothermal magnetization curve obtained at different temperatures. The so-called Maxwell relation gives an entropy change at designated temperatures by the formula of [39, 40]

$$\Delta S_M(T)_{\Delta H} = \mu_0 \int_{H_i}^{H_f} \left(\frac{\partial M(T, H)}{\partial T} \right)_H dH \quad (1)$$

where H_i is the initial field, H_f is the final field, and μ_0 is the vacuum permeability [5]. A decline in the degree of disorder in the magnetic moment distribution occurs with the increase of magnetic field, hence, ΔS_M turns to a negative value in this definition. Therefore, $-\Delta S_M$ is generally taken as one of the features to measure the MCE. Similarly, ΔT_{ad} can be visualized as the isentropic difference between the related total entropy $S_{\text{tot}}(T, H)$ functions associated with the demonstration of MCE, $dS = 0$ in terms of no change in the

Fig. 1 **a** Crystal structure of $\text{Gd}_{0.33}[\text{Gd}_4(\text{OH})_4(\text{OAc})_3][\text{Rh}_4\text{Zn}_4(\text{L-cys})_{12}] \cdot 32\text{H}_2\text{O}$ ($\mathbf{1}_{\text{Gd}}$) (L-cys = L-cysteinate) ($M_w = 3621.44 \text{ g mol}^{-1}$), **b** Packing structure in $\mathbf{1}_{\text{Gd}}$, **c** Schematic view of the Gd cubane cluster structure, **d** Lattice parameters and crystal symmetry of $\mathbf{1}_{\text{Gd}}$ and $\mathbf{2}_{\text{Gd}}$



total entropy because of adiabatic condition, then integrate the variations in the magnetic field [39]:

$$\Delta T_{\text{ad}} = -\mu_0 \int_{H_i}^{H_f} \frac{T}{C_p} \left(\frac{\partial M(T, H)}{\partial T} \right)_H dH \quad (2)$$

The heat capacity of $\mathbf{1}_{\text{Gd}}$ was measured by the thermal relaxation technique for a pellet sample of which total mass is 432.4 μg . The sample was pressed into a pellet and adhered to the sample stage using a small amount of Apiezon N grease to maintain thermal contact between the pellet and the sample stage. The background heat capacity including the grease was measured in a separate run and they were subtracted from the total heat capacity data obtained at each magnetic field. The integration of $C_p T^{-1}$ from the minimum temperature to 10 K and up to a maximum field of 5 T gives the temperature dependence of entropy. The measurement range of the heat capacity is from 0 to 5 T and the temperature interval is 0.9–10 K for each magnetic field. The lattice contribution has been evaluated by the Debye model approximation using the T^3 term of the nonmagnetic reference component of $\mathbf{1}_{\text{Gd}}$.

The direct variations of temperature induced by MCE were recorded using a homemade magnetocaloric cell designed for sub-mg samples of molecular compounds.

A similar method was performed by Korolev et al. in Ref. [41] for higher temperature regions near room temperature. Given that our molecular compounds show the MCE at extremely low temperature regions, we have developed a precise measurement system for small sample amounts on the order of 10^2 - μg . The cell is equipped with the ^3He probe and is available in variable temperature insert with a 9 T superconducting magnet. To realize an adiabatic environment, the sample cell is placed in a high vacuum below 0.1 mPa and heat loss through wires is minimized by using thin wires as leads. The temperature of thermal bath linked to the heat sink (T_b) is stabilized at a fixed temperature between 1.8 and 0.8 K by using ^4He or ^3He gas. The detailed structure of the cryostat is schematically shown in Fig. 2. Figure 3 represents a schematic drawing and photo picture of the magnetocaloric measurement system. The cell holder and the thermal bath are made of bakelite (polyoxybenzylmethylenglycolanhydride) owing to its insulating conductivity and relatively lower heat capacity [42], which can significantly suppress undesirable temperature rise induced by eddy currents in metals such as Cu and stainless by rapid field-sweeping [43, 44] of 1.7 T min^{-1} . As for the sample part, two ruthenium oxide chip-type resistors, RuO_x (1000 Ω at room temperature), were mounted at the center of the cell as thermometers, one was used for detecting the resistance and served as the platform of sample. The other sensor

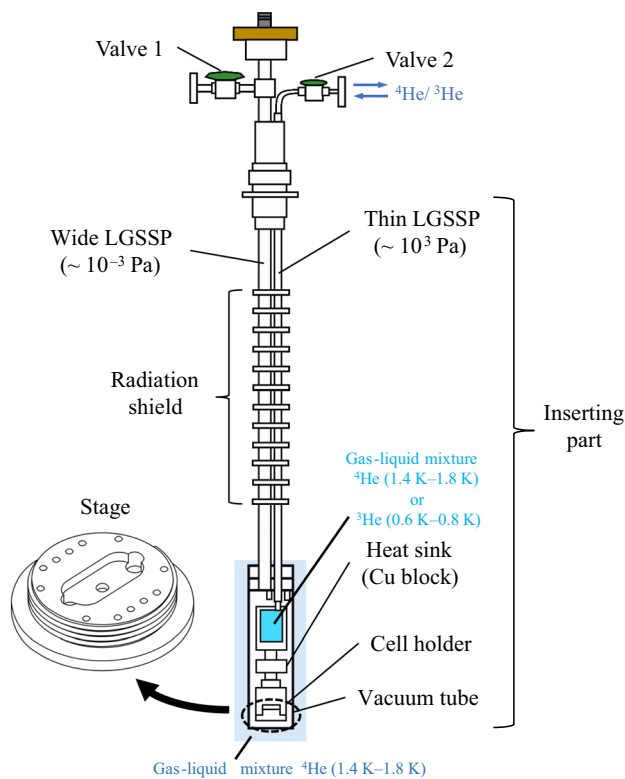


Fig. 2 Schematic of insert probe

was used as a reference, and the temperature differences between the sample (T_s) and the reference (T_r), denoted as ΔT ($\Delta T = T_s - T_r$), were detected. Both thermometers have weak thermal links with the heat sink through chromel wires ($\Phi = 13 \mu\text{m}$) that also work as leads for temperature detection. The wires were attached to the sensor by carbon paste and the contact parts were covered with epoxy to reinforce the bonding part instead of solder to avoid anomaly by the

superconductive transition of it during magnetic field sweep. To improve accuracy for measuring the resistance of the sensor, we cleaved the insulating parts of the chips made by Al_2O_3 down one-third of their original mass to minimize heat capacity and applied a sample in microgram amount for measurements. A calibrated CX-1030 resistance thermometer (LakeShore) was set at the bottom of the stage, aiming to control the bath temperature of the cell and to carry out the temperature calibration from the data obtained from these two chip-type resistors. We monitored these two thermometers by sweeping the magnetic field while keeping the base temperature almost constant, collected the temperatures of the two thermometers, and recorded their temperature difference ΔT . From the results of blank measurements from 0 to 5 T, no appreciable temperature difference was observed between them even at the relatively fast sweeping rate of 0.6 T min^{-1} , which means that the effects of the magnetic response of the addenda, such as Apiezon N grease, can be ignored. In this system, the signals were detected by model 370 AC resistance bridges (LakeShore) & model 340/350 temperature controllers (LakeShore).

Results and discussion

Figure 4a shows isothermal magnetization curves ($M-H$) of $\mathbf{1}_{\text{Gd}}$ obtained between 2 and 10 K with magnetic fields up to 7 T. The magnetization curves obey the Brillouin functions of $S=7/2$ in all temperature ranges which demonstrates that the Gd^{3+} ions are in paramagnetic state. Although a small decrease in χT is observed in the χT versus T plot below about 5 K, the paramagnetic Curie-temperature is about $\theta = -0.24 \text{ K}$ and there appears no magnetic ordering (In Fig. 5a). The experimental magnetic entropy change was then determined using the formula of Maxwell relation (Eq. 1) for the whole

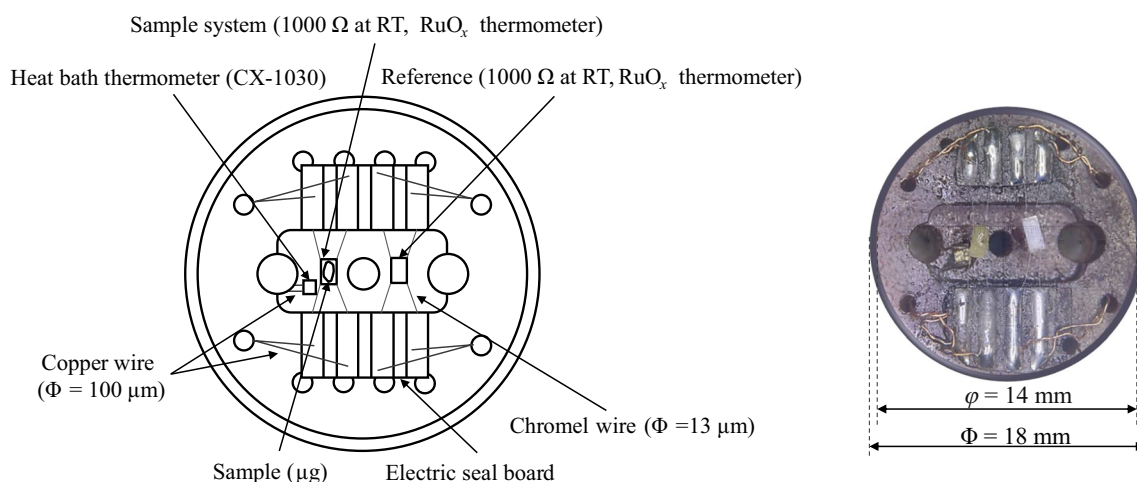


Fig. 3 Schematic of magnetocaloric measurement cell

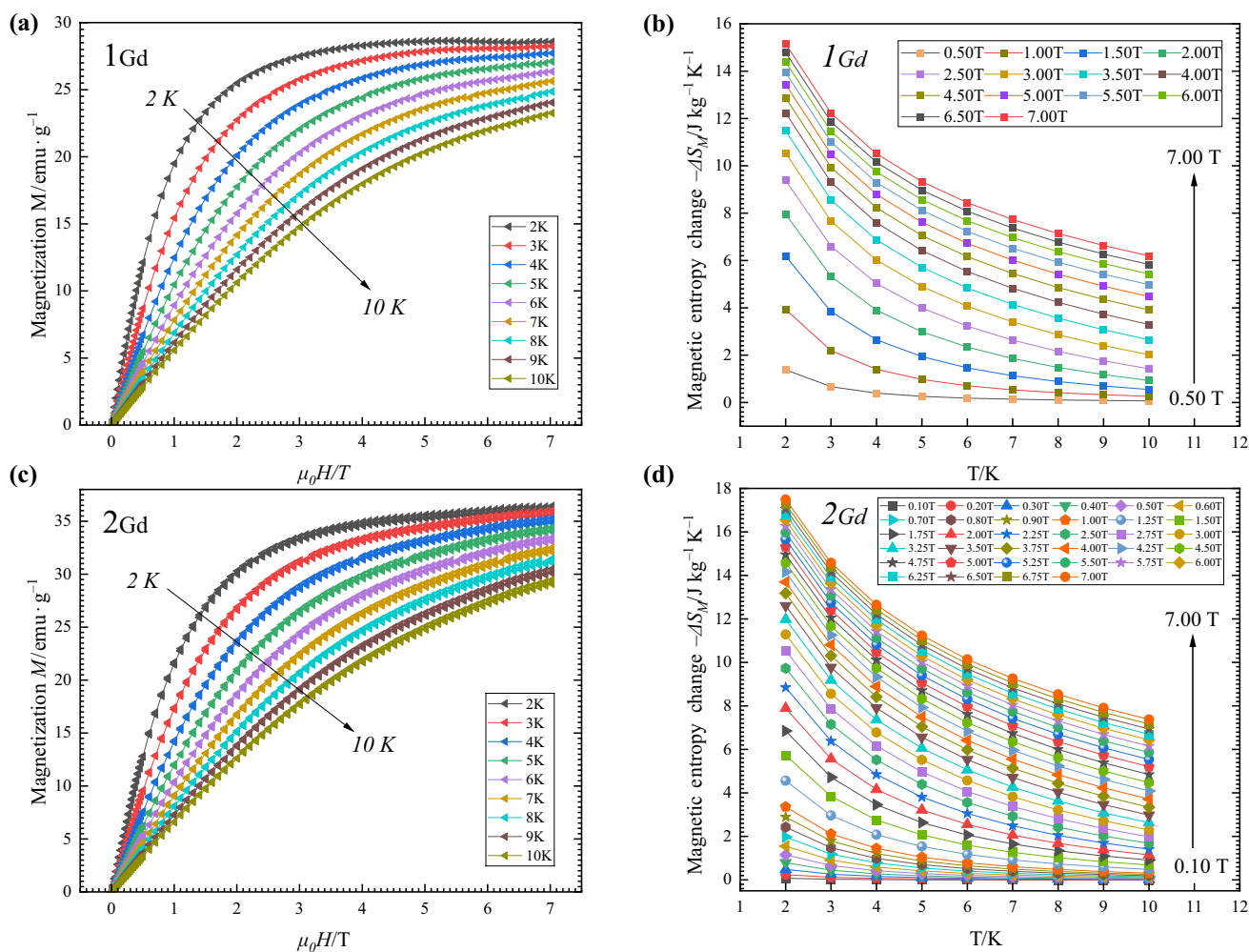


Fig. 4 **a** Isothermal magnetization M versus field $\mu_0 H$ for $\text{Gd}_{0.33}[\text{Gd}_4(\text{OH})_4(\text{OAc})_3][\text{Rh}_4\text{Zn}_4(\text{L-cys})_{12}]\cdot 32\text{H}_2\text{O}$ ($\mathbf{1}_{\text{Gd}}$), temperature from 2 to 10 K and field up to 7 T. **b** Temperature dependence of negative isothermal magnetic entropy change $-\Delta S_{\text{M}}(T)_{\Delta H}$ [Integral of Eq. (1)] for $\mathbf{1}_{\text{Gd}}$, as derived indirectly from isothermal mag-

netization data, **c** Isothermal magnetization M versus field $\mu_0 H$ $\text{Gd}_{0.33}[\text{Gd}_4(\text{OH})_4(\text{OAc})_3][\text{Ir}_4\text{Zn}_4(\text{L-cys})_{12}]\cdot 28\text{H}_2\text{O}$ ($\mathbf{2}_{\text{Gd}}$) temperature from 2 to 10 K and field up to 7 T. **d** Temperature dependence of negative isothermal magnetic entropy change $\Delta S_{\text{M}}(T)_{\Delta H}$ for $\mathbf{2}_{\text{Gd}}$

series from the isothermal magnetization curves we obtained. The results are shown in Fig. 4b. The red solid line and the squares represent the entropy change in the case of ΔH is 7 T ($\Delta S_{\text{M}}(T)_{7\text{T}}$), which indicates the maximum absolute value of the entropy change ($-\Delta S_{\text{M}}^{\text{max}}$) is $15.15 \text{ J kg}^{-1} \text{ K}^{-1}$ at 2.0 K. Figure 4c shows the isothermal magnetization curves of $\mathbf{2}_{\text{Gd}}$ compounds. The temperature dependence of χT and isothermal magnetization curves show a similar tendency with the first sample, although a slightly larger $\theta = -0.75 \text{ K}$ can be observed. The saturation of magnetization M (emu g^{-1}) near 7 T shows an almost equivalent tendency between two compounds. These facts indicate that the magnetic states of $\mathbf{1}_{\text{Gd}}$ and $\mathbf{2}_{\text{Gd}}$ are almost the same. The calculated $-\Delta S_{\text{M}}^{\text{max}}$ value of this compound is $17.49 \text{ J kg}^{-1} \text{ K}$ at 2.0 K as presented in Fig. 4d. The theoretical value of $-\Delta S_{\text{M}}^{\text{max}}$ can be evaluated

from the contribution of the uncoupled Gd^{3+} ions as [30, 45, 46]:

$$\Delta S_{\text{Gd}} = nR \ln(2S + 1) \quad (3)$$

where n accounts for the number of moles of Gd in $\mathbf{1}_{\text{Gd}}$, that is, $n_{\text{Gd}} = 4.33$, $S = 7/2$. Therefore, the theoretical value of $-\Delta S_{\text{M}}$ is $20.67 \text{ J kg}^{-1} \text{ K}^{-1}$. The experimental $-\Delta S_{\text{M}}$ of $\mathbf{1}_{\text{Gd}}$ achieves up to 73% of the ideal magnetic entropy change. In comparison, $\mathbf{2}_{\text{Gd}}$ reaches 91%, which indicates that the value of $\mathbf{2}_{\text{Gd}}$ is remarkably close to the theoretical value performing better MCE. The discrepancy between experimental and theoretical values may be ascribable to the weak antiferromagnetic interactions between the Gd^{3+} centers, as demonstrated in the Curie–Weiss analysis [47].

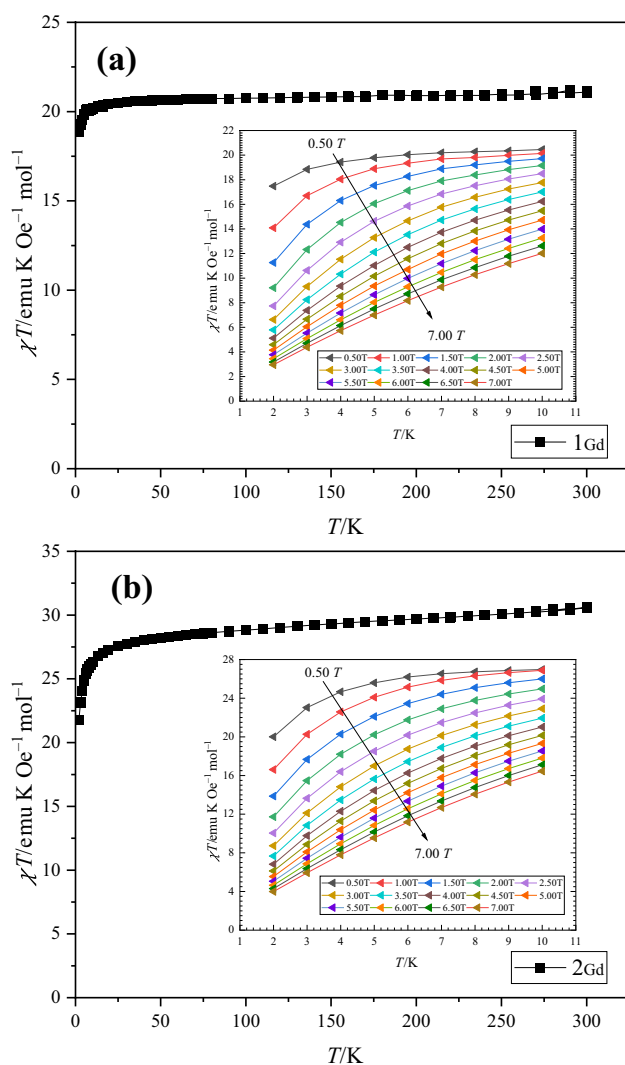


Fig. 5 The χT versus T plot of **a** $\mathbf{1}_{\text{Gd}}$ and **b** $\mathbf{2}_{\text{Gd}}$ ($H=1000$ Oe). A comparison of the χT versus T plots from 0.5 to 7 T derived from Fig. 4a [Inset of (a)] and Fig. 4c separately [Inset of (b)]

The variation of magnetic entropy available for MCE can be evaluated by the heat capacity measurements under magnetic fields up to 7 T. The temperature dependence of the heat capacity divided by temperature of $\mathbf{1}_{\text{Gd}}$ is described in Fig. 6a. The 0 T data shown by black color does not show any peaks in this temperature range which demonstrates that the absence of long-range orderings of spin down to the minimum temperature of 0.8 K in the present study. However, the small upturn of $C_p T^{-1}$ detected at low temperature regions below 3 K in the 0 T data suggesting that the release of magnetic entropy due to the degeneracy of $S=7/2$ spin occurs at a lower temperature range. This result certainly demonstrates that the ground state of compound $\mathbf{1}_{\text{Gd}}$ is kept as paramagnetic. The data with magnetic field of 1 T shown by the red dotted line reveals larger upturn compared to the case of 0 T. With increasing the magnetic field, $C_p T^{-1}$ shows

a peak structure that shifts to a higher temperature. This tendency can be explained by the Schottky heat capacity resulting from the Zeeman splitting of octahedral degeneracy. The magnetic entropy $S(T, H)$ can be calculated by integrating $C_p(T, H)T^{-1}$, and the temperature dependence of them are shown in Fig. 6b. The magnetic entropy data of the 0 T are not so clear as the extrapolation of the data is difficult. However, it is considered that the upturn should be the high-temperature tail of the Schottky anomaly and saturation entropy at higher temperatures is adjusted as the full entropy value of $4.33R\ln 8/M_{\mathbf{1Gd}}$ ($M_{\mathbf{1Gd}}=3621.44$ g mol $^{-1}$). Therefore, we show the entropy of 0 T data so as to reach $4.33R\ln 8/M_{\mathbf{1Gd}}$ at a higher temperature region in the plot. This temperature and magnetic field dependences of $\mathbf{1}_{\text{Gd}}$ demonstrate that the material is available for demagnetization cooling by using a large entropy difference between 0 and 3–5 T curves in the liquid helium temperature range.

In this section, we discuss the direct measurements of MCE results obtained using the system constructed in this work. The cooling experiments were performed under a high vacuum environment (less than 10^{-4} Pa) for $\mathbf{1}_{\text{Gd}}$ ($m=829.5$ μg) and $\mathbf{2}_{\text{Gd}}$ ($m=627.1$ μg), at various field cycles (0 T \rightarrow H \rightarrow 0 T) and two bath temperatures separately. With these experiments, it is possible to detect the heating/cooling due to the adiabatic change of the spin entropy in Gd^{3+} , namely, the decrease of entropy during the adiabatic conduction caused by the alignment of spins induces cooling of the sample. The results of temperature profiles during the magnetic field sweeping obtained for $\mathbf{1}_{\text{Gd}}$ and $\mathbf{2}_{\text{Gd}}$ samples are shown in Fig. 7; The black solid squares represent sample temperature while reference temperature is denoted by deep blue solid squares and the red solid squares stand for the values of the external magnetic field. A successive reduction in T_s as the result of MCE along with the demagnetization. The T_r do not change drastically since the reference cell only contains small amounts of magnetic impurities, i.e., some metal and a small amount of solder used as electrodes. During the de/magnetization process, the temperature of the heat sink made by bakelite is kept at a constant value (T_b) by a temperature controller (LakeShore model 350). By increasing the magnetic field, the temperature of the sample increases due to the decrease in magnetic entropy. The temperature gradually comes back to the original temperature due to the small heat leak by the lead wires (13 μm , chromel). The demagnetization process induces the decrease of temperature, and reaching the minimum temperature attained by adiabatic demagnetization.

The minimum temperatures attained by the sample of $\mathbf{1}_{\text{Gd}}$ are 0.45 K and 0.29 K from an initial temperature of 1.63 K with a field change of 3 T and 0.89 K with a field change of 2 T separately seen from Fig. 8a. The so-obtained $\Delta T_{\text{ad}} \cong 1.63-0.45$ K $\cong 1.18$ K, yielding a cooling

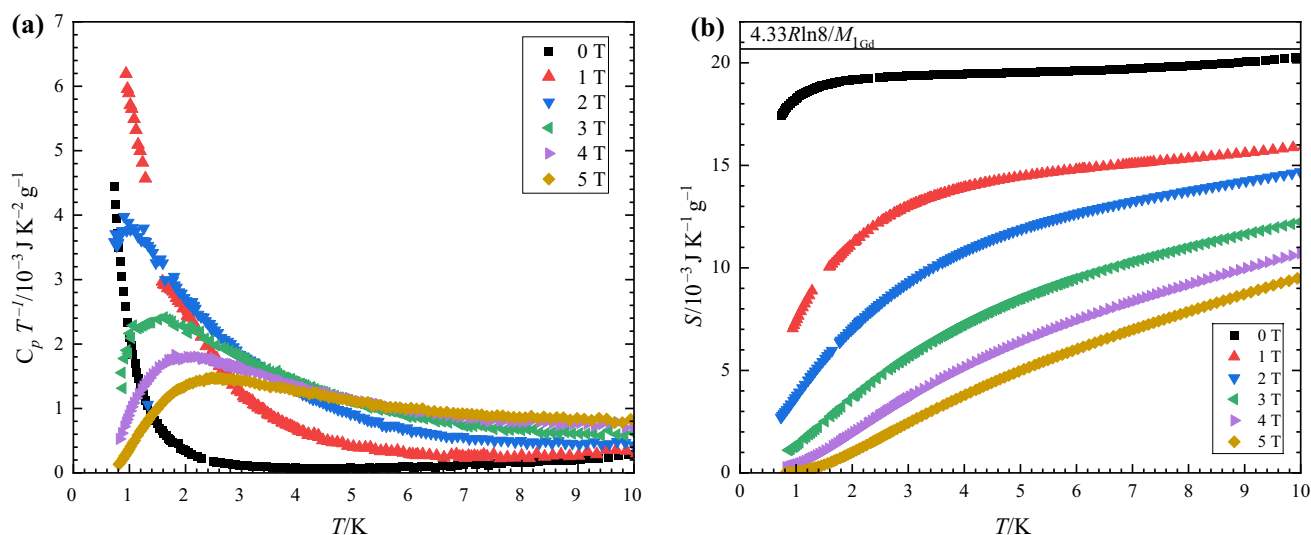


Fig. 6 **a** The magnetic heat capacity C_p of 1_{Gd} as a function of temperature and magnetic field, temperature intervals 1–10 K, field up to 5 T. **b** Magnetic entropy S_M calculated by integrating $C_p T^{-1}$. In zero-field, the entropy

is vertically shifted to match $4.33R\ln 8/M_{1\text{Gd}}$ ($M_{1\text{Gd}}=3621.44 \text{ g mol}^{-1}$)

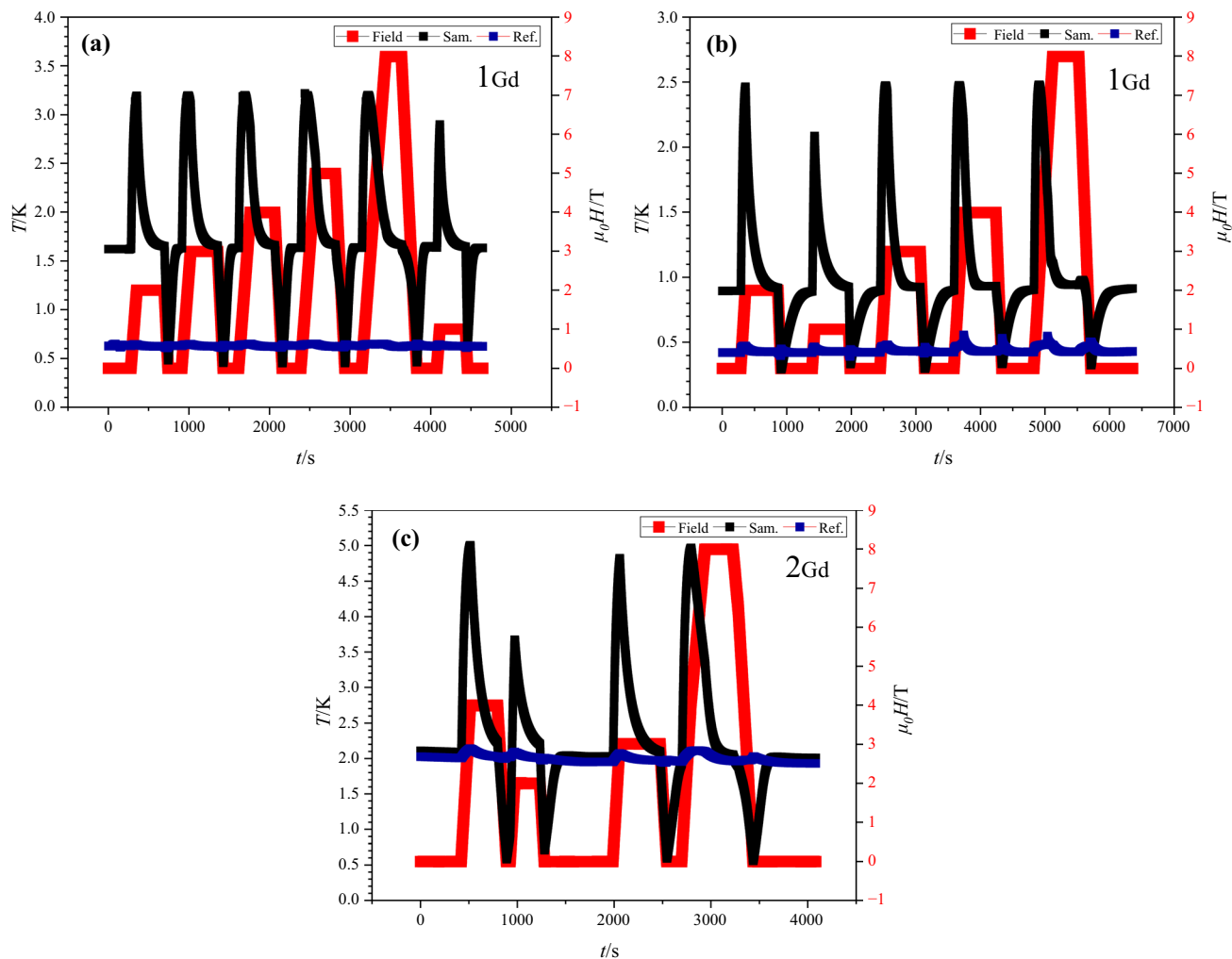


Fig. 7 Temperature variations of sample and reference cells occurred under field changes of $\Delta H=1, 2, 3, 4, 8 \text{ T}$. Experimental temperature changes of **a** sample 1_{Gd} in the adiabatic magnetic refrigeration pro-

cess at $T_b \approx 1.8 \text{ K}$ and **b** at $T_b \approx 0.8 \text{ K}$, **c** sample 2_{Gd} in the adiabatic magnetic refrigeration process at $T_b \approx 1.8 \text{ K}$

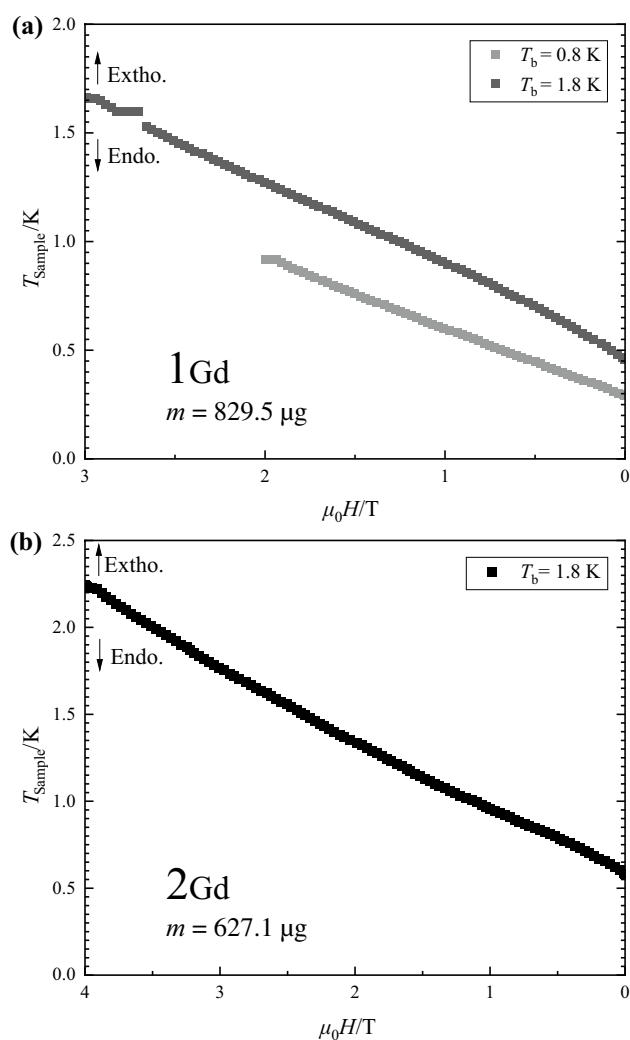


Fig. 8 Adiabatic change of sample temperatures as a function of the applied field on demagnetization. **a** Crystal $\mathbf{1}_{\text{Gd}}$ achieves at 450 mK and 290 mK from $T_i=1.63$ K and $H_i=3$ T and $T_i=0.89$ K and $H_i=2$ T initial conditions, respectively; (b) crystal $\mathbf{2}_{\text{Gd}}$ achieves at 580 mK from $T_i=2.10$ K and $H_i=4$ T initial conditions

rate (ν) of 0.39 K T^{-1} . In the latter case, ΔT_{ad} is approximately 0.6 K and the ν is 0.3 K T^{-1} . Figure 8b reveals the sample of $\mathbf{2}_{\text{Gd}}$ cools to 0.58 K when zero applied field from 2.1 K at 2 T. Its $\Delta T_{\text{ad}} \cong 1.52$ K, $\nu = 0.38$ K T^{-1} . Of note, the cooling effect, $\mathbf{2}_{\text{Gd}} \lesssim \mathbf{1}_{\text{Gd}}$ is not equivalent to the results from magnetization and heat-capacity analysis, nevertheless, it should be noted that the sample amount of $\mathbf{1}_{\text{Gd}}$ is 32.3% more than $\mathbf{2}_{\text{Gd}}$, and the cooling effect corresponds to the amounts of refrigerants. Moreover, the paramagnetic Curie-temperature of $\mathbf{2}_{\text{Gd}}$ is a slightly higher than $\mathbf{1}_{\text{Gd}}$, suggesting that $\mathbf{1}_{\text{Gd}}$ is more effective in maintaining the paramagnetic state than $\mathbf{2}_{\text{Gd}}$, especially below 1 K. Additionally, the base temperature stability in the case of $\mathbf{2}_{\text{Gd}}$ was not so good compared with $\mathbf{1}_{\text{Gd}}$ inferred from reference and bath temperature. Hence, we

cannot ensure enough accuracy for the data of sample $\mathbf{2}_{\text{Gd}}$ at present. However, by comparing the ΔT_{ad} curve and magnetic data, a similar tendency between $\mathbf{1}$ and $\mathbf{2}_{\text{Gd}}$ was observed.

We consider that the appearance of such large magnetocaloric effects in these two compounds may be attributed to the peculiar cubane structure of these materials. Although the Gd density is high in the cationic part of the crystals, the Gd^{3+} ions do not interact to form ordering since the Gd-cluster is frustrated which works to prohibit the long-range ordering. It is difficult to form a triangle or Kagome-type frustration frame by the Gd^{3+} due to the relatively large atomic radius, the cubane structure is more possible for lanthanide ions. Quite recently, a frustrated molecule-based material, $\text{Gd}(\text{OH})\text{SO}_4$, investigated by Han et al. [48] was observed with $-\Delta S_{\text{M}}^{\text{max}}$ of 53.5 J kg^{-1} K^{-1} for $\Delta H=7$ T and $T=2$ K, suggesting that the MCE is indeed enhanced by geometric frustration, however, no direct magnetocaloric measurements are available. Notable the materials also have network cubane structure.

Conclusions

We report the magnetic properties and thermodynamic properties of two frustrated lanthanide molecular compounds, $\text{Gd}_{0.33}[\text{Gd}_4(\text{OH})_4(\text{OAc})_3][\text{Rh}_4\text{Zn}_4(\text{L-cys})_{12}] \cdot 32\text{H}_2\text{O}$ ($\mathbf{1}_{\text{Gd}}$) and $\text{Gd}_{0.33}[\text{Gd}_4(\text{OH})_4(\text{OAc})_3][\text{Ir}_4\text{Zn}_4(\text{L-cys})_{12}] \cdot 28\text{H}_2\text{O}$ ($\mathbf{2}_{\text{Gd}}$) (L-cys = L-cysteinate), where the Gd^{3+} ions form cubane structure with frustrated structure. The frustrated configuration of Gd^{3+} spins in the cubane structure was found to lead to the low temperature paramagnetic state and prohibit the magnetic transition, as these systems remain paramagnetic at least down to 290 mK. The $-\Delta S_{\text{M}}^{\text{max}}$ of $\mathbf{1}_{\text{Gd}}$ and $\mathbf{2}_{\text{Gd}}$ determined by isothermal $M-H$ curve is determined to be 15.15 J kg^{-1} K^{-1} and 17.49 J kg^{-1} K^{-1} at 2.0 K under $\Delta H=7$ T, respectively, and the results of heat capacity of $\mathbf{1}_{\text{Gd}}$ are consistent with the magnetization characteristic. Direct detection of magnetocaloric effect by the newly constructed system reveals that the materials with this cubane network can attain extremely low temperatures below 1 K using the demagnetization range from 2 to 4 T.

Author contributions YZ and YN organized the work and performed experiments and led the physical discussion. They wrote a draft of the manuscript. TN designed the magnetocaloric system. SY performed magnetization measurement. HA attends the overall discussion. NY and TK synthesized crystals and performed crystallographic analysis. All authors confirmed and corrected the manuscript.

Funding Open Access funding provided by Osaka University. This work was partially supported by JSPS KAKENHI Grant Numbers: JP19K22169 and JP20H01862.

Declarations

Conflict of interest The authors declare they have no financial interests.

Open Access This article is licensed under a Creative Commons Attribution 4.0 International License, which permits use, sharing, adaptation, distribution and reproduction in any medium or format, as long as you give appropriate credit to the original author(s) and the source, provide a link to the Creative Commons licence, and indicate if changes were made. The images or other third party material in this article are included in the article's Creative Commons licence, unless indicated otherwise in a credit line to the material. If material is not included in the article's Creative Commons licence and your intended use is not permitted by statutory regulation or exceeds the permitted use, you will need to obtain permission directly from the copyright holder. To view a copy of this licence, visit <http://creativecommons.org/licenses/by/4.0/>.

References

- Lounasmaa OV, Parks RD. Experimental principles and methods below 1 K. *J Phys Today*. 1975;28:74–5. <https://doi.org/10.1063/1.3069146>.
- Pecharsky VK, Gschneidner KA Jr. Giant magnetocaloric effect in $Gd_5(Si_2Ge_2)$. *Phys Rev Lett*. 1997;78:4494–7. <https://doi.org/10.1103/PhysRevLett.78.4494>.
- Morrison K, Barcza A, Moore JD, Sandeman KG, Chattopadhyay MK, Roy SB, Caplin AD, Cohen LF. The magnetocaloric performance in pure and mixed magnetic phase $CoMnSi$. *J Phys D Appl Phys*. 2010;43: 195001. <https://doi.org/10.1088/0022-3727/43/19/195001>.
- Tegus O, Brück E, Buschow KH, De Boer FR. Transition-metal-based magnetic refrigerants for room-temperature applications. *Nature*. 2002;415:150–2. <https://doi.org/10.1038/415150a>.
- Tishin AM, Spichkin YI. The magnetocaloric effect and its applications. 1st ed. Boca Raton: CRC Press; 2003. <https://doi.org/10.1201/9781420033373>.
- Pecharsky VK, Gschneidner KA Jr. Magnetocaloric effect. In: Franco B, Gerald LL, Peter W, editors. *Encyclopedia of condensed matter physics*. Oxford: Elsevier; 2005. p. 236–44. <https://doi.org/10.1016/B0-12-369401-9/01127-X>.
- Smith A, Bahl CR, Bjørk R, Engelbrecht K, Nielsen KK, Pryds N. Materials challenges for high performance magnetocaloric refrigeration devices. *Adv Energy Mater*. 2012;2:1288–318. <https://doi.org/10.1002/aenm.201200167>.
- Buschow KHJ. Intermetallic compounds of rare-earth and 3d transition metals. *Rep Prog Phys*. 1977;40:1179. <https://doi.org/10.1088/0034-4885/40/10/002>.
- Givord DO, Lemaire RE. Magnetic transition and anomalous thermal expansion in R_2Fe_{17} compounds. *IEEE Trans Magn*. 1974;10:109–13. <https://doi.org/10.1109/TMAG.1974.1058311>.
- Palstra TTM, Mydosh JA, Nieuwenhuys GJ, Van der Kraan AM, Buschow KHJ. Study of the critical behaviour of the magnetization and electrical resistivity in cubic $La(Fe, Si)_{13}$ compounds. *J Magn Magn Mater*. 1983;36:290–6. [https://doi.org/10.1016/0304-8853\(83\)90128-2](https://doi.org/10.1016/0304-8853(83)90128-2).
- Brückner W, Perthel R, Kleinstück K, Schulze GE. Magnetic properties of $ZrFe_2$ and $TiFe_2$ within their homogeneity range. *Phys Status Solidi B Basic Res*. 1968;29:211–6. <https://doi.org/10.1002/pssb.19680290124>.
- Pieggger E, Craig RS. Structural and magnetic characteristics of $TiFe_2-ZrFe_2$ and $ZrCo_2-ZrFe_2$ alloys. *J Chem Phys*. 1963. <https://doi.org/10.1063/1.1733990>.
- Mukhamedov BO, Saenko I, Ponomareva AV, Kriegel MJ, Chugreev A, Udovsky A, Fabrichnaya O, Abrikosov IA. Thermodynamic and physical properties of Zr_3Fe and $ZrFe_2$ intermetallic compounds. *Intermetallics*. 2019;109:189–96. <https://doi.org/10.1016/j.intermet.2019.01.018>.
- Duc NH, Anh DTK. Magnetocaloric effects in RCo_2 compounds. *J Magn Magn Mater*. 2002;242–245:873–5. [https://doi.org/10.1016/S0304-8853\(01\)01328-2](https://doi.org/10.1016/S0304-8853(01)01328-2).
- Zhou KW, Zhuang YH, Li JQ, Deng JQ, Zhu QM. Magnetocaloric effects in $(Gd_{1-x}Tb_x)Co_2$. *Solid State Commun*. 2006;137:275–7. <https://doi.org/10.1016/j.ssc.2005.11.023>.
- Wang D, Liu H, Tang S, Yang S, Huang S, Du Y. Magnetic properties and magnetocaloric effects in $(Gd_xDy_{1-x})Co_2$ compounds. *Phys Lett A*. 2002;297:247–52. [https://doi.org/10.1016/S0375-9601\(02\)00159-7](https://doi.org/10.1016/S0375-9601(02)00159-7).
- Fujieda S, Fujita A, Fukamichi K. Large magnetocaloric effect in $La(Fe, Si_{1-x})_{13}$ itinerant-electron metamagnetic compounds. *Appl Phys Lett*. 2002;81:1276–8. <https://doi.org/10.1063/1.1498148>.
- Shen J, Wang F, Zhao JL, Wu JF, Gong MQ, Hu FX, Li YX, Sun JR, Shen BG. Reduction in hysteresis losses and large magnetic entropy change in the B-doped $La(Fe, Si)_{13}$ compounds. *J Appl Phys*. 2010;107:09A909. <https://doi.org/10.1063/1.3349325>.
- Xiang CH, Chen YG, Tang YB, Xiao DQ. Effect of Ce Co, B on formation of $LaCo_{13}$ -structure phase in $La(Fe, Si)_{13}$ alloys. *Trans Nonferrous Met Soc China*. 2014;24:705–11. [https://doi.org/10.1016/S1003-6326\(14\)63114-9](https://doi.org/10.1016/S1003-6326(14)63114-9).
- Dan'kov SY, Tishin AM, Pecharsky VK, Gschneidner KA Jr. Magnetic phase transitions and the magnetothermal properties of gadolinium. *Phys Rev B Condens Matter*. 1998;57:3478–90. <https://doi.org/10.1103/PhysRevB.57.3478>.
- Gompa TP, Greer SM, Rice NT, Jiang N, Telsler J, Ozarowski A, Stein BW, La Pierre HS. High-frequency and -field electron paramagnetic resonance spectroscopic analysis of metal-ligand covalency in a $4f^7$ valence series (Eu^{2+} , Gd^{3+} , and Tb^{4+}). *Inorg Chem*. 2021;60:9064–73. <https://doi.org/10.1021/acs.inorgchem.1c01062>.
- Giguere A, Foldeaki M, Gopal BR, Chahine R, Bose TK, Frydman A, Barclay JA. Direct measurement of the “giant” adiabatic temperature change in $Gd_5Si_2Ge_2$. *Phys Rev Lett*. 1999;83:2262–5. <https://doi.org/10.1103/PhysRevLett.83.2262>.
- Pecharsky VK, Gschneidner KA Jr. The giant magnetocaloric effect in $Gd_5(Si_xGe_{1-x})_4$ materials for magnetic refrigeration. In: Kittel P, editor. *Advances in cryogenic engineering*. Boston: Springer; 1998. p. 1729–36. https://doi.org/10.1007/978-1-4757-9047-4_218.
- Gschneidner Jr KA, Pecharsky VK, Pecharsky AO, Zimm CB. Recent developments in magnetic refrigeration. *Mater. Sci. Forum*. 1999;315:69–76. <https://doi.org/10.4028/www.scientific.net/MSF.315-317.69>.
- Pecharsky VK, Gschneidner KA Jr. $Gd_5(Si_xGe_{1-x})_4$: an extremum material. *Adv Mater*. 2001;13:683–6. [https://doi.org/10.1002/1521-4095\(200105\)13:9%3c683::AID-ADMA683%3e3.0.CO;2-O](https://doi.org/10.1002/1521-4095(200105)13:9%3c683::AID-ADMA683%3e3.0.CO;2-O).
- Pecharsky VK, Samolyuk GD, Antropov VP, Pecharsky AO, Gschneidner KA Jr. The effect of varying the crystal structure on the magnetism, electronic structure and thermodynamics in the $Gd_5(Si_xGe_{1-x})_4$ system near $x = 0.5$. *J Solid State Chem*. 2003;171:57–68. [https://doi.org/10.1016/S0022-4596\(02\)00146-9](https://doi.org/10.1016/S0022-4596(02)00146-9).

27. Evangelisti M, Brechin EK. Recipes for enhanced molecular cooling. *Dalton Trans.* 2010;39:4672–6. <https://doi.org/10.1039/B926030G>.
28. Falsaperna M, Saines PJ. Development of magnetocaloric coordination polymers for low temperature cooling. *Dalton Trans.* 2022;51:3394–410. <https://doi.org/10.1039/D1DT04073A>.
29. Zhuo Z, Li GL, Huang YG. Understanding magneto-structural correlations toward design of molecular magnets. In: Cao, R, editor. *Advanced Structural Chemistry*. New Jersey: Wiley-VCH; 2021. p. 777–832. <https://doi.org/10.1002/9783527831753.ch13>.
30. Silva RS Jr, Gainza J, dos Santos C, Rodrigues JE, Dejoie C, Huttel Y, Biskup N, Nemes NM, Martínez JL, Ferreira NS, Alonso JA. Magnetoelastic coupling and cryogenic magnetocaloric effect in two-site disordered GdSrCoFeO₆ double perovskite. *Chem Mater.* 2023;35:2439–55. <https://doi.org/10.1021/acs.chemmater.2c03574>.
31. Roubeau O, Natividad E, Evangelisti M, Lorusso G, Palacios E. A magnetocaloric composite based on molecular coolers and carbon nanotubes with enhanced thermal conductivity. *Mater Horiz.* 2017;4:464–76. <https://doi.org/10.1039/C6MH00533K>.
32. Luo XM, Hu ZB, Lin QF, Cheng W, Cao JP, Cui CH, Mei H, Song Y, Xu Y. Exploring the performance improvement of magnetocaloric effect based Gd-exclusive cluster Gd₆₀. *J Am Chem Soc.* 2018;140:11219–22. <https://doi.org/10.1021/jacs.8b07841>.
33. Lidiard AB. Antiferromagnetism. *Rep Prog Phys.* 1954;17:201. <https://doi.org/10.1088/0034-4885/17/1/307>.
34. Hou YS, Xiang HJ, Gong XG. Lattice-distortion Induced magnetic transition from low-temperature antiferromagnetism to high-temperature ferrimagnetism in double perovskites A₂FeOsO₆ (A = Ca, Sr). *Sci Rep.* 2015;5:13159. <https://doi.org/10.1038/srep13159>.
35. Yoshinari N, Meundaeng N, Tabe H, Yamada Y, Yamashita S, Nakazawa Y, Konno T. Single-crystal-to-single-crystal installation of Ln₄(OH)₄ cubanes in an anionic metallosupramolecular framework. *Angew Chem Int Ed.* 2020;59:18048–53. <https://doi.org/10.1002/anie.202008296>.
36. Anwar MU, Al-Harrasi A, Rawson JM, Gavey EL, Regier J, Alexandropoulos D, Pilkington M, Thompson LK. Slow magnetic relaxation in Dy₂ and Dy₄ complexes of a versatile, trifunctional polydentate N, O-ligand. *Dalton Trans.* 2019;48:14269–78. <https://doi.org/10.1039/C9DT02331C>.
37. Windsor HJ, Kepert CJ, Macreadie LK. Spontaneous resolution of two chiral metal–organic frameworks through local geometric and lattice frustration effects. *CrystEngComm.* 2023;25:5428–35. <https://doi.org/10.1039/D3CE00784G>.
38. Thammakan S, Yoshinari N, Tsuchikawa M, Rujiwatra A, Konno T. Postsynthetic installation of lanthanide cubane clusters in a 3D hydrogen-bonded framework of Ir^{III}₄Zn^{II}₄ multicarboxylates. *Inorg Chem.* 2024;63:6239–47. <https://doi.org/10.1021/acs.inorgchem.3c04513>.
39. Morrish AH. *The physical principles of magnetism*. 1st ed. New Jersey: Wiley 1965.
40. Pecharsky VK, Gschneidner KA Jr. Magnetocaloric effect from indirect measurements: magnetization and heat capacity. *J Appl Phys.* 1999;86:565–75. <https://doi.org/10.1063/1.370767>.
41. Korolev VV, Korolev DV, Ramazanova AG. The calorimetric method of evaluating the performance of magnetocaloric materials. *J Therm Anal Calorim.* 2019;136:937–41. <https://doi.org/10.1007/s10973-018-7704-y>.
42. Kumar N, Kumar P, Sharma M. Reconfigurable antenna and performance optimization approach. *Wirel Pers Commun.* 2020;112:2187–212. <https://doi.org/10.1007/s11277-020-07145-0>.
43. Imajo S, Dong C, Matsuo A, et al. High-resolution calorimetry in pulsed magnetic fields. *Rev Sci Instrum.* 2021;92: 043901. <https://doi.org/10.1063/5.0040655>.
44. Mejía CS, Niehoff T, Straßheim M, Bykov E, Skourski Y, Wosnitza J, Gottschall T. On the high-field characterization of magnetocaloric materials using pulsed magnetic fields. *J Phys Energy.* 2023;5: 034006. <https://doi.org/10.1088/2515-7655/acd47d>.
45. Koskelo EAC, Liu C, Mukherjee P, Kelly ND, Dutton SE. Free-spin dominated magnetocaloric effect in dense Gd³⁺ double perovskites. *Chem Mater.* 2022;34:3440–50. <https://doi.org/10.1021/acs.chemmater.2c00261>.
46. Xu LY, Zhao JP, Liu T, Liu FC. Gadolinium sulfate modified by formate to obtain optimized magneto-caloric effect. *Inorg Chem.* 2015;54:5249–56. <https://doi.org/10.1021/acs.inorgchem.5b00214>.
47. Li Y, Gegenwart P, Tsirlin AA. Spin liquids in geometrically perfect triangular antiferromagnets. *J Phys Condens Matter.* 2020;32: 224004. <https://doi.org/10.1088/1361-648X/ab724e>.
48. Han Y, Han SD, Pan J, Ma YJ, Wang GM. An excellent cryogenic magnetic cooler: magnetic and magnetocaloric study of an inorganic frame material. *Mater Chem Front.* 2018;2:2327–32. <https://doi.org/10.1039/C8QM00439K>.

Publisher's Note Springer Nature remains neutral with regard to jurisdictional claims in published maps and institutional affiliations.